


Dynamics of Circumstellar Planets in Binary Star Systems

Man Hoi Lee^{1,2} , Ka Ho Wong¹, Ho Wan Cheng¹, Trifon Trifonov³,
Sabine Reffert⁴ and Andreas Quirrenbach⁴

¹Department of Earth Sciences, The University of Hong Kong, Pokfulam Road, Hong Kong
email: mhlee@hku.hk

²Department of Physics, The University of Hong Kong, Pokfulam Road, Hong Kong

³Max-Planck-Institut für Astronomie, Königstuhl 17, 69117 Heidelberg, Germany

⁴Landessternwarte, Zentrum für Astronomie der Universität Heidelberg,
Königstuhl 12, 69117 Heidelberg, Germany

Abstract. Circumstellar planets in binary star systems provide unique constraints on the formation and dynamical evolution of planets. We present an empirical formula for the stability boundary of coplanar retrograde orbits, similar to the classic one for coplanar prograde orbits. We discuss two of the tightest binaries with circumstellar planets: HD 59686 and ν Octantis. For HD 59686, dynamical fitting of the radial velocity data and stability analysis show that the planet must be either on a nearly coplanar retrograde orbit or in one of the narrow regions of prograde orbits stabilized by secular apsidal alignment. For ν Octantis, a nearly coplanar retrograde planetary orbit is the only option for dynamical stability. We also discuss the mysterious case of ϵ Cygni. It shows short-period radial velocity variations that closely resemble the signal of a Jupiter-mass planet, but the period and amplitude change over time and dynamical stability analysis rules out a planet.

Keywords. planets - binary stars - stability - HD59686 - ν Octantis

1. Planets in Binary Star Systems

Planets in binary star systems provide unique constraints on the formation and dynamical evolution of planets. They can be orbiting around one of the stars in a circumstellar (S-type) orbit or around the binary in a circumbinary (P-type) orbit (Dvorak 1986). To date, the number of detected planets in binary star systems is only about 440, even though nearly 1/3 of nearby solar-type stars are in binary systems (Duquennoy and Mayor 1991; Raghavan et al. 2010) and the number of confirmed exoplanets is over 5500 (see <https://exoplanetarchive.ipac.caltech.edu/>). The small detection number of these planets is in part due to observational bias. But observations have also shown that the planet occurrence rate in binary systems with orbital semimajor axis $a_B \lesssim 47$ AU is only $\sim 34\%$ of that for wider binaries or single stars (Wang et al. 2014a,b; Kraus et al. 2016).

Figure 1 shows the orbital semimajor axis of the outermost planet versus the projected separation or semimajor axis (if orbit is known) of the binary for all binaries of separation < 500 AU with circumstellar planets. The filled square and triangle are the ν Octantis and HD 59686 systems, respectively, with the horizontal bars indicating the periastron and apastron binary separations. They are two of the tightest binaries ($a_B \lesssim 20$ AU) with circumstellar planets on relatively wide orbits ($a_p \gtrsim 1$ AU), and in both cases, the planet is likely on retrograde orbit relative to the binary's. We examine these systems in this

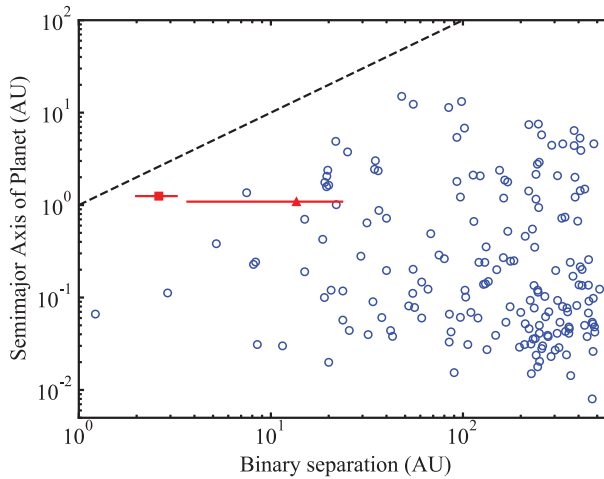


Figure 1. Orbital semimajor axis of the outermost planet versus the projected separation or semimajor axis (if the orbit is known) of the binary for all binaries of separation < 500 AU with circumstellar planets. Data obtained from http://exoplanet.eu/planets_binary/.

paper, after we discuss the stability boundary of circumstellar orbits in binary systems and the mysterious case of ϵ Cygni.

2. Stability of Circumstellar Orbits in Binary Systems

In the classic work by [Holman and Wiegert \(1999\)](#), the stability of both circumstellar and circumbinary planetary orbits was studied by performing numerical simulations for a wide range of binary mass ratio $\mu_B = M_B / (M_A + M_B)$ and eccentricity e_B (see also [Rabl and Dvorak 1988](#); [Quarles and Lissauer 2016](#); [Quarles et al. 2020](#)). The system consists of a primary star of mass M_A and a secondary star of mass M_B in an orbit of semimajor axis a_B and a test particle in a coplanar, prograde, and initially circular orbit (i.e., orbital angular momentum of the test particle is parallel to that of the binary) at semimajor axis a_p . For each combination of μ_B and e_B , the stability boundary for circumstellar planets is defined as a_p where all orbits with $a_p < a_{c,pro}$ are stable for 10^4 binary periods. By fitting an empirical formula to the numerical results, [Holman and Wiegert \(1999\)](#) obtained the following formula for the stability boundary of coplanar prograde orbits:

$$a_{c,pro}/a_B = 0.464 - 0.380\mu_B - 0.631e_B + 0.586\mu_B e_B + 0.150e_B^2 - 0.198\mu_B e_B^2. \quad (1)$$

It should be noted that the boundary between stable and unstable regions is not sharp and that there is a transition region between $a_{c,pro}$ and a second boundary at $a_{c,2,pro} > a_{c,pro}$ where some orbits are stable.

It is well known since the work by [Harrington \(1977\)](#) that retrograde orbits are more stable than prograde ones (see also [Morais and Giuppone 2012](#); [Quarles and Lissauer 2016](#)), but as far as we know, an empirical formula similar to Equation (1) had not been constructed. We have performed numerical simulations using the Wisdom-Holman symplectic integrator in the SWIFT package with setup similar to those of [Holman and Wiegert \(1999\)](#), but for coplanar, retrograde, and initially circular test particle orbits (see [Wong & Lee](#), in preparation, for details). The results are shown in the left panel of [Figure 2](#). As expected, systems with a more massive perturber (i.e., larger μ_B) and/or larger e_B have smaller $a_{c,retro}$. We apply a least-squares fit to the results and

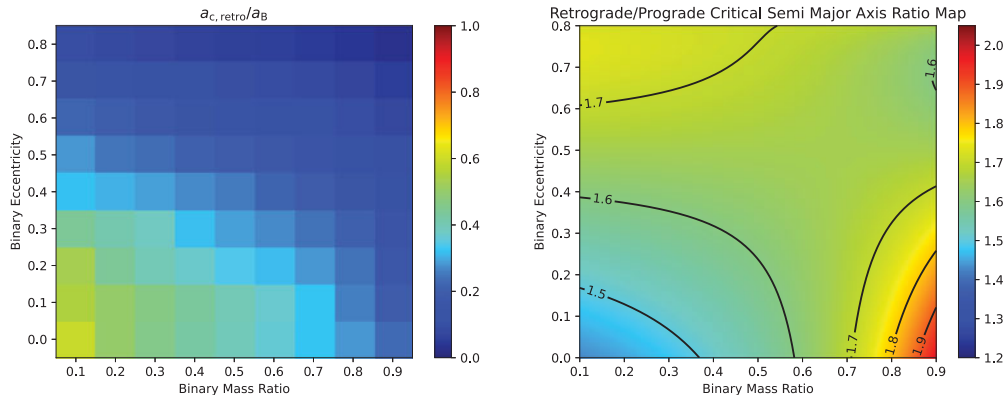


Figure 2. Stability boundary $a_{c,\text{retro}}/a_B$ (left panel) and the ratio $a_{c,\text{retro}}/a_{c,\text{pro}}$ (right panel) in the parameter space of the binary mass ratio μ_B and eccentricity e_B .

obtain the following formula for the stability boundary of coplanar retrograde orbits:

$$a_{c,\text{retro}}/a_B = 0.654 - 0.456\mu_B - 0.684e_B + 0.418\mu_B e_B - 0.0182e_B^2 + 0.0855\mu_B e_B^2. \quad (2)$$

The ratio $a_{c,\text{retro}}/a_{c,\text{pro}}$, using Equations (1) and (2), is shown in the right panel of Figure 2. The ratio $a_{c,\text{retro}}/a_{c,\text{pro}}$ is larger than one over the whole region, which means that retrograde orbits are more stable than prograde orbits for general binary systems. The ratio $a_{c,\text{retro}}/a_{c,\text{pro}}$ is conveniently nearly constant (≈ 1.5 – 1.7) over a wide range of μ_B and e_B relevant for circumstellar planets in binary star systems. In the Hill's regime where $\mu = 1 - \mu_B = M_A/(M_A + M_B) \ll 1$ and $e_B = 0$, we find that $a_{c,\text{retro}}/a_{c,\text{pro}} \approx 2$. Further analysis shows that both $a_{c,\text{pro}}$ and $a_{c,\text{retro}}$ scale with the Hill radius $r_H = (\mu/3)^{1/3}a_B$, with $a_{c,\text{pro}} \approx 0.45r_H$ and $a_{c,\text{retro}} \approx 0.92r_H$ (see also [Innanen 1980](#); [Hamilton and Burns 1991, 1992](#)).

3. A Cautionary Tale: ϵ Cygni

[Heeren et al. \(2021\)](#) have analyzed in detail the radial velocity (RV) observations of ϵ Cygni, which is a K0 III giant star of $M_A = 1.10M_\odot$. ϵ Cygni was observed by the Lick G and K giants RV survey ([Frink et al. 2001](#); [Reffert et al. 2015](#)). The Lick RV measurements and earlier RV measurements by [McMillan et al. \(1992\)](#) show a long term trend due to a distant binary companion and short-period (~ 290 d) variations that could be due to a circumstellar planet orbiting the primary star. A large set of RVs was subsequently obtained with the SONG telescope from 2015 to 2018. The stellar companion happened to go through periastron passage during this time, which allows the properties of the highly eccentric binary to be accurately determined: $a_B = 15.8$ AU, $e_B = 0.93$, and the minimum mass of the secondary $M_B \sin i = 0.265M_\odot$. If the short-period RV variations were due to a planet, the best double-Keplerian fit indicates that the planet would have an orbital period of about 291 d, $a_p = 0.89$ AU, and a minimum mass of $1.0M_J$, where M_J is Jupiter mass. However, a more careful analysis shows that both the period and amplitude of the short-period variations change over time. In addition, a planet at $a_p \sim 0.89$ AU should be unstable according to Equations (1) and (2), and it would come within the Hill radius of the stellar companion at periastron distance $q_B \sim 1.1$ AU. A more detailed stability analysis of this system confirms that no stable orbits could be found in a large region of parameter space around the best fit. So it is highly unlikely that the short-period RV variations are due to a planet. The most likely explanation for the short-period variations of ϵ Cygni is the heartbeat phenomenon, which are stellar oscillations excited by a stellar companion passing close to the primary. But it would be a rather extreme example of a

heartbeat system, because of its large periastron separation (> 20 stellar radii) and large stellar radius ($\approx 11R_{\odot}$).

4. HD 59686

HD 59686 is another star observed by the Lick G and K giants RV survey. It is a K2 III giant star of $M_A = 1.9M_{\odot}$. The 88 RV measurements over 12 years clearly show a circumstellar planet on a nearly circular orbit around the primary star of an eccentric binary, with the double-Keplerian fit giving $M_B \sin i = 0.530M_{\odot}$, $P_B = 11700$ d, $a_B = 13.6$ AU, $e_B = 0.729$, $M_p \sin i = 6.9M_J$, $P_p = 299$ d, $a_p = 1.09$ AU, and $e_p = 0.05$ (Ortiz et al. 2016). HD 59686 is the most eccentric close binary to harbor a circumstellar planet. The high binary eccentricity means that the stars are only separated by ~ 3.7 AU at periastron, leading to strong gravitational perturbations of the planet at $a_p = 1.09$ AU by the secondary. Indeed, a_p is just outside the stability boundary for coplanar prograde orbits, which is $a_{c,\text{pro}} \approx 0.97$ AU according to Equation (1). On the other hand, a_p is well inside the stability boundary for coplanar retrograde orbits, which is $a_{c,\text{retro}} \approx 1.67$ AU according to Equation (2).

Trifonov et al. (2018) have performed a detailed orbital and stability analysis of this system. The best coplanar prograde dynamical fit is unstable on timescales of about 42 kyr. The best coplanar retrograde dynamical fit is slightly better than the prograde dynamical fit in χ^2 value, and it is stable for at least 10 Myr. A bootstrap analysis finds that a few % of the edge-on prograde dynamical fits are stable, while almost all of the edge-on retrograde dynamical fits are stable for at least 10 Myr. The stable prograde fits fall in narrow regions of the parameter space, and they are stabilized by secular apsidal alignment, with the difference in the longitude of periape $\Delta\varpi = \varpi_p - \varpi_B$ librating about 0°

4.1. Stability of Planetary Orbits in HD 59686

Chan & Lee (in preparation) have explored systematically the parameter space of planetary orbits in the HD 59686 system to investigate its stability behaviors, particularly those related to secular apsidal alignment and mean-motion resonances (MMR). The planet is treated as a test particle in a circumstellar orbit around the primary star. We use the Wisdom-Holman symplectic integrator in the SWIFT package for the numerical simulations, and the maximum integration time is 10^5 binary periods.

Figure 3 shows the numerical results on the survival time of the particles in the (a_p, e_p) parameter space for coplanar prograde orbits with initial $\Delta\varpi = 0^\circ$ and mean anomalies $\mathcal{M}_p = 0^\circ$ and $\mathcal{M}_B = 180^\circ$. There is a bulk stable region in the lower left corner that shrinks toward smaller semimajor axis at higher eccentricity, which is expected because more eccentric orbits are generally less stable. The stability boundary, which is the boundary of the bulk stable region at $e_p = 0$, is $a_{c,\text{pro}} = 0.975$ AU, which is in good agreement with 0.97 AU from Equation (1). Other than the bulk stable region, we see two new stability features. The first feature is the set of stable islands at $e_p \sim 0.1$ that extend from $a_p \approx 0.95$ AU to $a_p \approx 1.1$ AU. They exist at distances beyond the circular stability boundary $a_{c,\text{pro}}$. They fall on a nearly horizontal line but break apart at the positions of MMR. These stable islands are due to secular apsidal alignment. The second feature is the set of stable islands at the odd-order MMR such as 1:40, 1:42, 1:44, and 1:46 at 1.072, 1.038, 1.006, and 0.977 AU, respectively. These stable islands also exist at distances beyond the circular stability boundary $a_{c,\text{pro}}$, and they are at higher eccentricities than the secular apsidal alignment islands. Figure 4 is similar to Figure 3, but for simulations with the planet initially at its apocenter ($\mathcal{M}_p = 180^\circ$). The islands stabilized by secular apsidal alignment are similar, but the MMR stable islands are at even orders (1:39, 1:41, etc.).

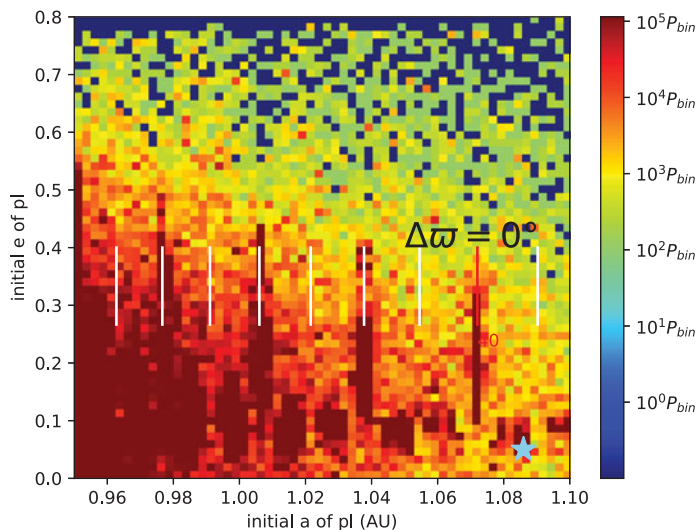


Figure 3. Stability map of the HD 59686 system showing the time at which a test particle becomes unstable as a function of initial a_p and e_p for coplanar prograde orbits with initial $\Delta\varpi = 0^\circ$, $\mathcal{M}_p = 0^\circ$, $\mathcal{M}_B = 180^\circ$. The best-fit (a_p, e_p) of the observed planet is indicated by the star. Positions of MMR are indicated by the vertical lines, with the red one for 1:40.

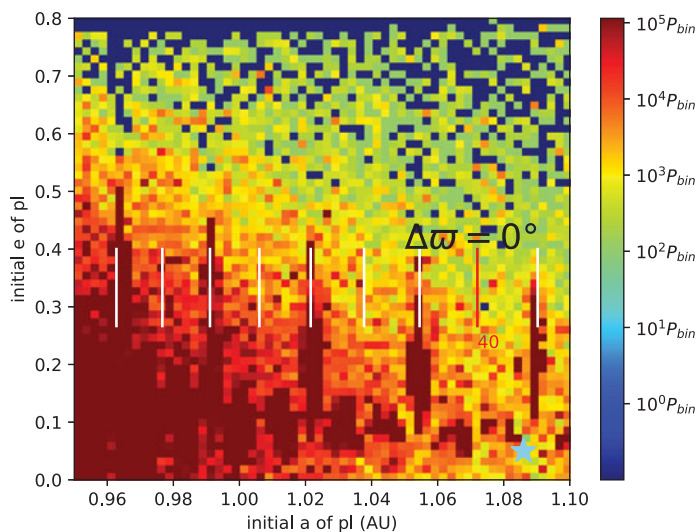


Figure 4. Same as Figure 3, but with initial $\Delta\varpi = 0^\circ$, $\mathcal{M}_p = 180^\circ$, $\mathcal{M}_B = 180^\circ$.

The different patterns are due to the different initial \mathcal{M}_p , which leads to different initial MMR angles.

Figure 5 is similar to Figure 3 but for coplanar retrograde planetary orbits. The planetary orbits are initially aligned with the binary orbit ($\Delta\varpi = 0^\circ$), with $\mathcal{M}_p = 0^\circ$ and $\mathcal{M}_B = 180^\circ$. The bulk stable region in the lower left corner is significantly larger than that for prograde orbits in Figure 3, with the stability boundary $a_{c,\text{retro}} = 1.5$ AU, which is slightly smaller than 1.67 AU from Equation (2). Besides the bulk stable region, there is a series of islands stabilized by secular apsidal alignment that extend from the bulk region to the right along a nearly horizontal line at $e_p \sim 0.25$, and there are also stable

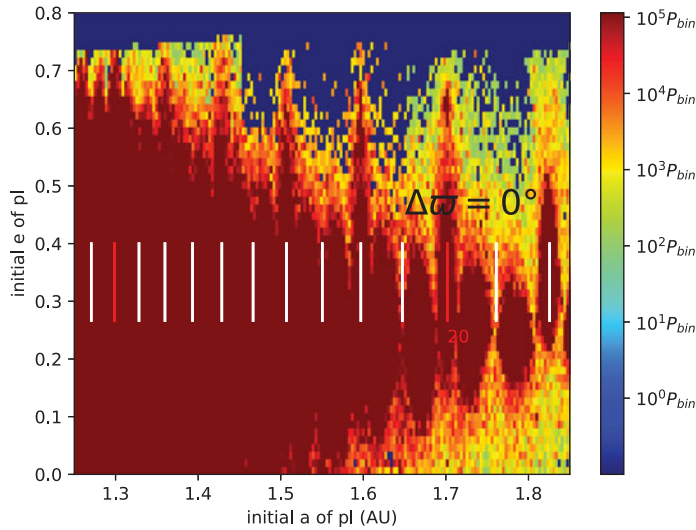


Figure 5. Same as Figure 3, but for coplanar retrograde orbits with initial $\Delta\varpi = 0^\circ$, $\mathcal{M}_p = 0^\circ$, $\mathcal{M}_B = 180^\circ$. The red vertical lines indicate the 1:20 and 1:30 MMR.

islands at higher e_p at the odd-order MMR such as 1:18, 1:20, 1:22, etc. As in the case of prograde orbits, simulations with the same initial $\Delta\varpi = 0^\circ$ and $\mathcal{M}_B = 180^\circ$ as Figure 5 but $\mathcal{M}_p = 180^\circ$ show similar stable islands due to secular apsidal alignment but MMR stable islands at even orders. The range of a_p simulated and shown in Figure 5 is chosen such that it covers well the stability boundary ($a_{c,retro}$) and one can see the details of the transition from the stable region to the unstable region. The observed planet at $a_p = 1.09$ AU and $e_p = 0.05$ sits well inside the bulk stable region to the left of the region shown in Figure 5.

Based on these results, we can conclude that the real planet is more likely to be in a retrograde configuration, because coplanar retrograde orbits have a much larger stable region around the real planet's position than coplanar prograde orbits. If the real planet is in a prograde configuration, it must be in one of the narrow islands stabilized by secular apsidal alignment (in particular, the ones just inside and outside the 1:39 MMR, which are within the 1σ errors of the observed parameters), and it must not be in MMR with the binary companion, because the stable islands due to MMR have much higher e_p than the observed value.

5. ν Octantis

The planet in the ν Octantis system is undoubtedly one of the most dynamically challenging circumstellar planets in binary star systems. It was originally discovered by Ramm et al. (2009) based on ~ 220 cross-correlation (CCF) RV measurements taken with the HERCULES spectrograph on the 1-m telescope at Mt John Observatory. The data show evidence for a circumstellar planet and a binary companion around the K1 III giant star of $M_A = 1.6M_\odot$, with $M_B \sin i \approx 0.50M_\odot$, $P_B \approx 1050$ d, $a_B \approx 2.5$ AU, $e_B \approx 0.23$, $M_p \sin i \approx 2.4M_J$, $P_p \approx 417$ d, $a_p \approx 1.2$ AU, and $e_p \approx 0.12$. The planetary orbit is located at almost twice the distance of the prograde stability boundary of $a_{c,pro} \approx 0.65$ AU from Equation (1). Thus, the planet could not possibly be in a nearly coplanar and prograde orbit: it is in a highly unstable region of parameter space, which is unlikely to have any orbits stabilized by secular apsidal alignment or MMR (as in the case of HD 59686). On the other hand, a_p is comparable to the retrograde stability boundary of

$a_{c,retro} \approx 1.0$ AU from Equation (2), and Eberle and Cuntz (2010), Quarles *et al.* (2012), and Goździewski *et al.* (2013) have shown that the planet could be in a nearly coplanar and retrograde orbit.

Ramm *et al.* (2016) have subsequently obtained an additional ~ 1200 RV measurements with higher precision in 2009–2013 using an iodine cell with the HERCULES spectrograph. The RV data continues to show the short-period signal. A careful analysis of the photospheric and chromospheric activity indicators has also found no significant RV-correlated variability (Ramm *et al.* 2021). We have recently obtained new HARPS RV data, which together with the previous data, show that the short-period signal has been coherent for over 16 periods, which strongly suggests that the planet is real.

Finally, the mass of the secondary star is $M_B = 0.57M_{\odot}$ (with inclination $i_B = 71.8^{\circ}$ from HIPPARCOS data), which means that it could be either a low-mass main-sequence star or a white dwarf. We have obtained VLT/SPHERE adaptive optics image that could help us answer this question. If the secondary star is a white dwarf, then it is initially the more massive star and the evolution of the binary would have significant implications for the origin and evolution of the planet. A detailed analysis of the RV and imaging data will be reported in a forthcoming article (Cheng *et al.*, in preparation).

6. Summary

Although it is important to keep in mind that nearly periodic RV variations of a star may not be due to an orbiting planet, as in the case of ϵ Cygni, there is strong evidence that the RV signals for the circumstellar planets in the HD 59686 and ν Octantis binary systems are real. HD 59686 and ν Octantis are two of the tightest binaries with circumstellar planets, and the planets are most likely on retrograde orbits, which are stable out to larger orbital semimajor axis than prograde orbits. For HD 59686, although we cannot yet rule out that the planet is on a prograde orbit, one would have to explain how a planet could be formed in a narrow region of the parameter space stabilized by secular apsidal alignment. If the circumstellar planets in both of these systems are confirmed to be on retrograde orbit, they pose serious challenging questions to the theory of planet formation: Did these planets form in retrograde circumstellar disk? Were they captured from prograde circumbinary orbits into retrograde circumstellar orbits (Gong and Ji 2018)? Are they the result of binary evolution?

Acknowledgements. This work was supported in part by Hong Kong RGC grants 17305015 and 17306720.

References

- Duquennoy, A. & Mayor, M. 1991, *A&A*, 248, 485–524.
 Dvorak, R. 1986, *A&A*, 167, 379–386.
 Eberle, J. & Cuntz, M. 2010, *ApJL*, 721, L168–L171.
 Frink, S., Quirrenbach, A., Fischer, D., Röser, S., & Schilbach, E. 2001, *PASP*, 113, 173–187.
 Gong, Y.-X. & Ji, J. 2018, *MNRAS*, 478, 4565–4574.
 Goździewski, K., Słonina, M., Migaszewski, C., & Rozenkiewicz, A. 2013, *MNRAS*, 430, 533–545.
 Hamilton, D. P. & Burns, J. A. 1991, *Icarus*, 92, 118–131.
 Hamilton, D. P. & Burns, J. A. 1992, *Icarus*, 96, 43–64.
 Harrington, R. S. 1977, *AJ*, 82, 753–756.
 Heeren, P., Reffert, S., Trifonov, T., Wong, K. H., Lee, M. H., Lillo-Box, J., Quirrenbach, A., Arentoft, T., Albrecht, S., Grundahl, F., Andersen, M. F., Antoci, V., & Pallé, P. L. 2021, *A&A*, 647, A160.
 Holman, M. J. & Wiegert, P. A. 1999, *AJ*, 117, 621–628.
 Innanen, K. A. 1980, *AJ*, 85, 81–85.
 Kraus, A. L., Ireland, M. J., Huber, D., Mann, A. W., & Dupuy, T. J. 2016, *AJ*, 152, 8.

- McMillan, R. S., Smith, P. H., Moore, T. L., & Perry, M. L. 1992, *PASP*, 104, 1173.
- Morais, M. H. M. & Giuppone, C. A. 2012, *MNRAS*, 424, 52–64.
- Ortiz, M., Reffert, S., Trifonov, T., Quirrenbach, A., Mitchell, D. S., Nowak, G., Buenzli, E., Zimmerman, N., Bonnefoy, M., Skemer, A., Defrère, D., Lee, M. H., Fischer, D. A., & Hinz, P. M. 2016, *A&A*, 595, A55.
- Quarles, B., Cuntz, M., & Musielak, Z. E. 2012, *MNRAS*, 421, 2930–2939.
- Quarles, B., Li, G., Kostov, V., & Haghighipour, N. 2020, *AJ*, 159, 80.
- Quarles, B. & Lissauer, J. J. 2016, *AJ*, 151, 111.
- Rabl, G. & Dvorak, R. 1988, *A&A*, 191, 385–391.
- Raghavan, D., McAlister, H. A., Henry, T. J., Latham, D. W., Marcy, G. W., Mason, B. D., Gies, D. R., White, R. J., & ten Brummelaar, T. A. 2010, *ApJS*, 190, 1–42.
- Ramm, D. J., Nelson, B. E., Endl, M., Hearnshaw, J. B., Wittenmyer, R. A., Gunn, F., Bergmann, C., Kilmartin, P., & Brogt, E. 2016, *MNRAS*, 460, 3706–3719.
- Ramm, D. J., Pourbaix, D., Hearnshaw, J. B., & Komonjinda, S. 2009, *MNRAS*, 394, 1695–1710.
- Ramm, D. J., Robertson, P., Reffert, S., Gunn, F., Trifonov, T., Pollard, K., & Cantalloube, F. 2021, *MNRAS*, 502, 2793–2806.
- Reffert, S., Bergmann, C., Quirrenbach, A., Trifonov, T., & Künstler, A. 2015, *A&A*, 574, A116.
- Trifonov, T., Lee, M. H., Reffert, S., & Quirrenbach, A. 2018, *AJ*, 155, 174.
- Wang, J., Fischer, D. A., Xie, J.-W., & Ciardi, D. R. 2014,a *ApJ*, 791a, 111.
- Wang, J., Xie, J.-W., Barclay, T., & Fischer, D. A. 2014,b *ApJ*, 783b, 4.